Check for updates

cScience

WILEY | 有科出版 YOUKE PUBLISHING

RESEARCH ARTICLE OPEN ACCESS

On the Use of Dispersion Corrections by Default in Computational Catalysis

Mahdiyeh Gholami[1,2] | Ricardo Urrego-Ortiz[1,3] | Mahdi Pourfath[4] | Stefan Kurth[1,5,6] | Federico Calle-Vallejo[1,5]

[1]Nano-Bio Spectroscopy Group and European Theoretical Spectroscopy Facility (ETSF), Department of Polymers and Advanced Materials: Physics, Chemistry and Technology, University of the Basque Country EHU, San Sebastián, Spain | [2]School of Electrical and Computer Engineering, College of Engineering, University of Tehran, Tehran, Iran | [3]Department of Materials Science and Chemical Physics & Institute of Theoretical and Computational Chemistry (IQTCUB), University of Barcelona, Barcelona, Spain | [4]Institute for Microelectronics/E360, Vienna, Austria | [5]IKERBASQUE, Basque Foundation for Science, Bilbao, Spain | [6]Donostia International Physics Center (DIPC), San Sebastián, Spain

Correspondence: Federico Calle-Vallejo (federico.calle@ehu.es)

Received: 2 June 2026 | **Accepted:** 14 July 2026

Keywords: adsorbed-phase corrections | CO adsorption | density functional theory | dispersion corrections | gas-phase corrections

ABSTRACT

Accurate adsorption energy predictions are central in computational catalysis. The need for higher accuracy without prohibitive computational costs has led to the development of correction schemes for density functional theory (DFT) predictions. For instance, dispersion corrections are nowadays routinely applied, even when long-range interactions are expected to be negligible. To evaluate this practice, we assess the effects of D3 dispersion corrections on CO adsorption over transition metals using the Perdew–Burke–Ernzerhof (PBE) and revised PBE (RPBE) exchange-correlation functionals. These corrections systematically stabilize the CO adsorption energies, which generally increases deviations from experimental data. Furthermore, depending on the damping function used (zero or Becke–Johnson damping), D3 corrections alter the gas-phase thermochemistry. However, applying both gas- and adsorbed-phase corrections yields adsorption energies that closely match experimental values. Consequently, the application of dispersion corrections by default may compromise the predictive capability of DFT-based models.

1 | Introduction

Carbon monoxide (CO) is a representative gas and adsorbed species in catalysis, frequently acting as a reactant, product, and intermediate in numerous processes. For example, in heterogeneous catalysis, CO is used in methanol synthesis [1], Fischer–Tropsch synthesis [2], and the water–gas shift reaction [3]. In electrocatalysis, the electroreduction of CO (and carbon dioxide (CO_2)) is promising for addressing climate change while producing value-added chemicals such as methane, ethylene, and ethanol [4, 5], whereas CO oxidation is a widely studied model reaction [6–8] with clear implications for direct methanol and ethanol fuel cells [9–11]. In these reactions, CO adsorption or desorption frequently plays a key role in the overall catalytic activity. Therefore, the inaccurate prediction of CO adsorption energies impairs the capacity of computational chemistry models to explain existing experimental observations, suggest additional experiments, or guide the rational design of novel catalysts [12].

Although density functional theory (DFT) is one of the most widespread tools in computational chemistry [13, 14], and a vast array of exchange-correlation functionals are available [15], those based on the generalized gradient approximation (GGA), such as the Perdew–Burke–Ernzerhof (PBE) [16], the revised PBE by Hammer et al. (RPBE) [17], and the Bayesian error estimation functional with van der Waals correlation (BEEF–vdW) [18], remain the most prevalent in catalytic modeling. Although these functionals are computationally efficient, systematic errors persist, such as the well-documented

This is an open access article under the terms of the Creative Commons Attribution License, which permits use, distribution and reproduction in any medium, provided the original work is properly cited.

© 2026 The Author(s). *cScience* is copyright © Youke Publishing Co., Ltd.

"CO puzzle" [19], which can be resolved by employing more sophisticated functionals [20], DFT + U [21], or higher-level approaches such as the random phase approximation [22]. Other prominent limitations include the description of $O_{2(g)}$ [23], solid oxide thermochemistry [24–26], hydroxyl adsorption on metals [27], oxygen adsorption on RuO_2 [28, 29], and various other chemical systems [30, 31].

A major limitation of GGA functionals is their insufficient description of long-range interactions [32]. The dispersion corrections developed by Grimme et al. [33–36] are added to DFT calculations to improve the modeling of these interactions. Specifically, D3 corrections were designed to swiftly improve the accuracy of standard DFT by adding a semi-empirical dispersion energy term to the total energy of the system [37]. However, it remains unclear whether dispersion corrections are necessary to reliably predict adsorption energies. In fact, dispersion corrections are often added by default to improve the modeling of weak interactions [38–40]. However, this may not always be advisable, especially for a strong chemisorbate such as CO, which is ubiquitous in catalysis [1–11].

In this study, CO adsorption on various transition metals is evaluated using the PBE and RPBE functionals, both with and without D3 dispersion corrections. D3 corrections generally increased the PBE and RPBE deviations of the CO adsorption energies relative to the experimental results, suggesting that dispersion corrections must be used with caution, particularly for strongly chemisorbed species. To rationally improve the predictive capabilities of the evaluated functionals toward chemical accuracy, a scheme is proposed to mitigate both gas- and adsorbed-phase errors.

2 | Experimental

2.1 | Computational Settings

DFT calculations were performed using the Vienna ab initio simulation package (VASP) [41, 42] with the PBE [16] and RPBE [17] functionals. The projector augmented-wave (PAW) method was used to describe the interactions between the core ions and valence electrons [43, 44]. Zero damping and Becke–Johnson damping D3 dispersion corrections (denoted D3 (ZD) and D3(BJ), respectively) were incorporated via the method developed by Grimme et al. [37] as implemented in VASP. A plane-wave cutoff energy of 450 eV was used in all calculations.

The metal surfaces in this study were modeled using a (2 × 2) supercell of face-centered cubic (111) and (100) facets, utilizing the optimized lattice parameters listed in Supporting Information S1: Table S1. Specifically, Ni, Pt, Pd, Ir, Cu, and Rh were modeled using their face-centered cubic (111) facets; the Pd (100) facet was also included. For Co and Ru, the hexagonal close-packed (hcp) (0001) surface orientation was employed. All slabs consisted of four atomic layers, with the exception of Pd (100), which was modeled with five layers. In all cases, the two bottom-most atomic layers remained fixed at the optimized bulk distances, whereas the remaining layers and adsorbates were allowed to fully relax in all directions during the structural optimization performed using the conjugate-gradient algorithm. Spin-unrestricted calculations were performed for Co and Ni. Supporting Information S1: Figure S2 shows a schematic model of the (111) slab illustrating the investigated adsorption sites.

A (6 × 6 × 1) Monkhorst–Pack *k*-point grid [45] was employed to sample the reciprocal space for the slab calculations. The electronic states near the Fermi level were treated using the Methfessel–Paxton smearing method [46] using a width of 0.2 eV, and the final total energies were extrapolated to 0 K. All slabs and adsorbed species were relaxed until the forces on any atom were below 0.05 eV/Å. Urrego-Ortiz et al. [47] proved that reducing the force threshold from 0.05 to 0.01 eV/Å resulted in negligible differences in the CO adsorption energies. $CO_{(g)}$ was relaxed in a 15 × 15 × 15 $Å^3$ cubic box using the conjugate-gradient algorithm, sampling only the Γ-point until the forces on the atoms were below 0.01 eV/Å. Gaussian smearing was employed with an electronic temperature of 0.001 eV, and the total energy was extrapolated to 0 K.

2.2 | DFT-Based Adsorption Enthalpies

The enthalpy of species *i* (H_i^{DFT}) can be approximated from DFT calculations as follows:

$$H_i^{DFT} \approx E_i^{DFT} + ZPE_i \quad (1)$$

where E_i^{DFT} is the total energy and ZPE_i is the zero-point energy. The ZPE is calculated via vibrational frequency analysis within the harmonic oscillator approximation; for slabs with adsorbed CO, only the adsorbate contributions were considered (see Supporting Information S1: Tables S2 and S12). Thermal contributions are omitted from Equation (1) to facilitate direct comparison with the pioneering work of Wellendorff et al. [48] and because previous studies have shown that these contributions remain negligible from 0 to 298.15 K for numerous chemical reactions [49]. The adsorption enthalpy (ΔH_{CO}^{DFT}) is estimated by applying Equation (2) to the adsorption process: $* + CO_{(g)} \rightarrow *CO$, where the asterisk represents a free active site on the metal and *CO denotes the adsorbed species.

$$\Delta H_{CO}^{DFT} = \Delta E_i^{DFT} + \Delta ZPE_i \quad (2)$$

In Equation (2), Δ is the difference between the products and reactants of the corresponding quantities accounting for the respective stoichiometric coefficients. Supporting Information S1: Table S2 lists the calculated ZPE values used to estimate these adsorption enthalpies and Supporting Information S1: Table S3 lists the resulting adsorption enthalpies calculated for all scrutinized functionals.

2.3 | Experimental Adsorption Enthalpies

The experimental CO adsorption enthalpies of the transition metals were extracted from the study by Wellendorff et al. [48]. These results correspond to low-coverage adsorption configurations in which *CO did not dissociate and were obtained using different techniques, including single-crystal adsorption calorimetry, temperature-programmed desorption, and equilibrium adsorption isotherms. The arithmetic average was used for systems in which multiple experimental values were reported.

30676630, 2026, 3, Downloaded from https://onlinelibrary.wiley.com/doi/10.1002/csc3.70031 by Technische Universitaet Wien, Wiley Online Library on [23/09/2026]. See the Terms and Conditions (https://onlinelibrary.wiley.com/terms-and-conditions) on Wiley Online Library for rules of use; OA articles are governed by the applicable Creative Commons License

Supporting Information S1: Table S4 lists the experimental data and the techniques employed to measure them.

2.4 | Errors in the DFT Energies of Molecules and Adsorbates

To clarify terminology, the term "correction" is applied herein to two distinct concepts: dispersion corrections and gas- or adsorbed-phase corrections. The former term refers to the explicit inclusion of dispersion interactions within DFT energies, whereas the latter involves the modification of DFT total energies to align with experimental thermochemistry data for molecules and adsorbed species.

Urrego-Ortiz et al. [47] reported that ΔH_{CO}^{DFT} for transition metals deviates significantly from the experimental enthalpies (ΔH_{CO}^{exp}) across multiple functionals. The total deviation from experimental values (ε^T) originates from the cumulative errors in the thermochemical descriptions of the adsorbate, adsorbent, and free molecule, as expressed in Equation (3):

$$\varepsilon^T = (\varepsilon_{*CO} - \varepsilon_*) - \varepsilon_{CO_{(g)}} = \Delta H_{CO}^{DFT} - \Delta H_{CO}^{exp} \quad (3)$$

where ε_{*CO} is the error associated with the adsorbed CO and adsorbent, and ε_* is the error of the adsorbent. Hence, $(\varepsilon_{*CO} - \varepsilon_*)$ is the error of adsorbed CO, hereafter represented as $\overline{\varepsilon_{CO}}$ for brevity. Furthermore, $\varepsilon_{CO_{(g)}}$ is the error within the DFT-calculated energy of $CO_{(g)}$. Notably, $\varepsilon_{CO_{(g)}}$ can be derived from the $CO_{(g)}$ formation energy [30, 50], whereas $\overline{\varepsilon_{CO}}$ can be estimated using experimental adsorption energies [27, 47, 48]. Supporting Information S1: Note S1 details the calculation of these errors. Equation (4) shows that the gas-phase error can be included to yield an enthalpy with gas-phase corrections (ΔH_{CO}^{GPC}), whereas Equation (5) provides an adsorption enthalpy with gas- and adsorbed-phase corrections ($\Delta H_{CO}^{GPC+APC}$) that rectifies both the gas- and adsorbed-phase errors.

$$\Delta H_{CO}^{GPC} = \Delta H_{CO}^{DFT} + \varepsilon_{CO_{(g)}} \quad (4)$$

$$\Delta H_{CO}^{GPC+APC} = \Delta H_{CO}^{DFT} + \left(\varepsilon_{CO_{(g)}} - \overline{\varepsilon_{CO}}\right) \quad (5)$$

In principle, if $\varepsilon_{CO_{(g)}}$ and $\overline{\varepsilon_{CO}}$ are determined directly by comparing DFT values with experimental values without any fitting or averaging procedures, then $\Delta H_{CO}^{GPC+APC} = \Delta H_{CO}^{exp}$. However, fitting and averaging procedures among similar catalysts and/or families of compounds (such as nitrogen oxides (N_xO_y)) is a common practice [47, 51, 52]. Consequently, the final errors are not exactly zero, yet they remain considerably smaller than the initial deviations, with the average deviations typically being below 0.10 eV ($\left|\Delta H_{CO}^{GPC+APC} - \Delta H_{CO}^{exp}\right| < 0.10$ eV).

3 | Results and Discussion

3.1 | D3 Dispersion Corrections on CO Adsorption

Dispersion corrections should be used in systems where long-range interactions either dominate or contribute significantly to the physical and chemical properties of interest. Representative examples include (i) graphite, where the constituent layers are bound via van der Waals interactions [53], (ii) liquid water [54], and (iii) physisorption phenomena, such as the adsorption of water [55, 56], alkane, benzene [48], and graphene [57, 58] on metal surfaces. Furthermore, although the solvation energies of chemisorbates in water have been shown to be functional-dependent [59], systematic comparisons with experimental values remain scarce in the literature.

To address whether dispersion corrections are generally required to describe adsorption phenomena, Figure 1 shows parity plots comparing the calculated adsorption enthalpies of $CO_{(g)}$ on various transition metals. These calculations were performed using PBE both with and without D3 corrections (ΔH_{CO}^{PBE-D3} and ΔH_{CO}^{PBE}, respectively), as well as RPBE with and without D3 corrections ($\Delta H_{CO}^{RPBE-D3}$ and ΔH_{CO}^{RPBE}, respectively). Figure 1A,B shows the parity plots for PBE with D3(ZD) and D3(BJ) corrections, respectively ($\Delta H_{CO}^{PBE-D3(ZD)}$ and $\Delta H_{CO}^{PBE-D3(BJ)}$), whereas Figure 1C,D shows the corresponding results for the RPBE functional ($\Delta H_{CO}^{RPBE-D3(ZD)}$ and $\Delta H_{CO}^{RPBE-D3(BJ)}$). In all cases, the regression lines exhibit slopes close to unity but are shifted downward relative to the parity line ($y = x$), which indicates that the D3-corrected functionals generally produce more negative CO adsorption energies than the standard functionals.

The average stabilization of the PBE-D3-calculated adsorption energies relative to the plain PBE functional is indicated by the offsets in Figure 1, yielding values of 0.22 and 0.27 eV for the D3(ZD) and D3(BJ) methods, respectively. This finding is consistent with a previous report of 0.23 eV for PBE-D3(ZD) [47]. In contrast, the RPBE functional exhibits larger offsets, with stabilizations of 0.33 and 0.86 eV for the D3(ZD) and D3(BJ) corrections, respectively. Notably, in addition to the substantial adsorption energy differences introduced by the D3(BJ) damping, this scheme also modifies the *CO adsorption sites on Ni(111), Pd(100), Co(0001), and Ru(0001) relative to both the plain RPBE and RPBE-D3(ZD) calculations (see Supporting Information S1: Table S5).

The CO adsorption enthalpy can be expressed as $\Delta H_{CO}^{DFT} = \left(\Delta_f H_{*CO} - \Delta_f H_*\right) - \Delta_f H_{CO_{(g)}}$, where the term in parentheses represents the solid-phase contribution, $\Delta_f H_{CO_{(g)}}$ is the gas-phase contribution, and the subindex f indicates that $\Delta_f H$ is a formation enthalpy. Because the PBE-calculated formation enthalpies of $CO_{(g)}$ with and without D3 corrections are nearly identical ($\Delta_f H_{CO(g)}^{PBE} \approx \Delta_f H_{CO(g)}^{PBE-D3(ZD)} \approx \Delta_f H_{CO(g)}^{PBE-D3(BJ)}$), the D3 corrections primarily alter the solid-phase thermochemistry predictions of PBE. A similar behavior is observed for RPBE-D3(ZD), where the zero-damping formation enthalpies closely match those obtained with plain RPBE. However, when BJ damping is employed, the computed $\Delta_f H_{CO_{(g)}}$ differs by 0.31 eV between RPBE and RPBE-D3(BJ), indicating that the stabilization induced by this damping scheme cannot be ascribed solely to changes in the solid-phase thermochemistry. Supporting Information S1: Table S6 lists the $CO_{(g)}$ formation enthalpies across all evaluated scenarios.

3.2 | Comparison With Experimental Energies

As previously mentioned, prior studies have revealed notable deviations between DFT predictions of adsorption energies and experimental benchmarks [48]. These findings challenge the widespread assumption that the DFT-calculated energies of

30676630, 2026, 3, Downloaded from https://onlinelibrary.wiley.com/doi/10.1002/csc3.70031 by Technische Universitaet Wien, Wiley Online Library on [23/09/2026]. See the Terms and Conditions (https://onlinelibrary.wiley.com/terms-and-conditions) on Wiley Online Library for rules of use; OA articles are governed by the applicable Creative Commons License

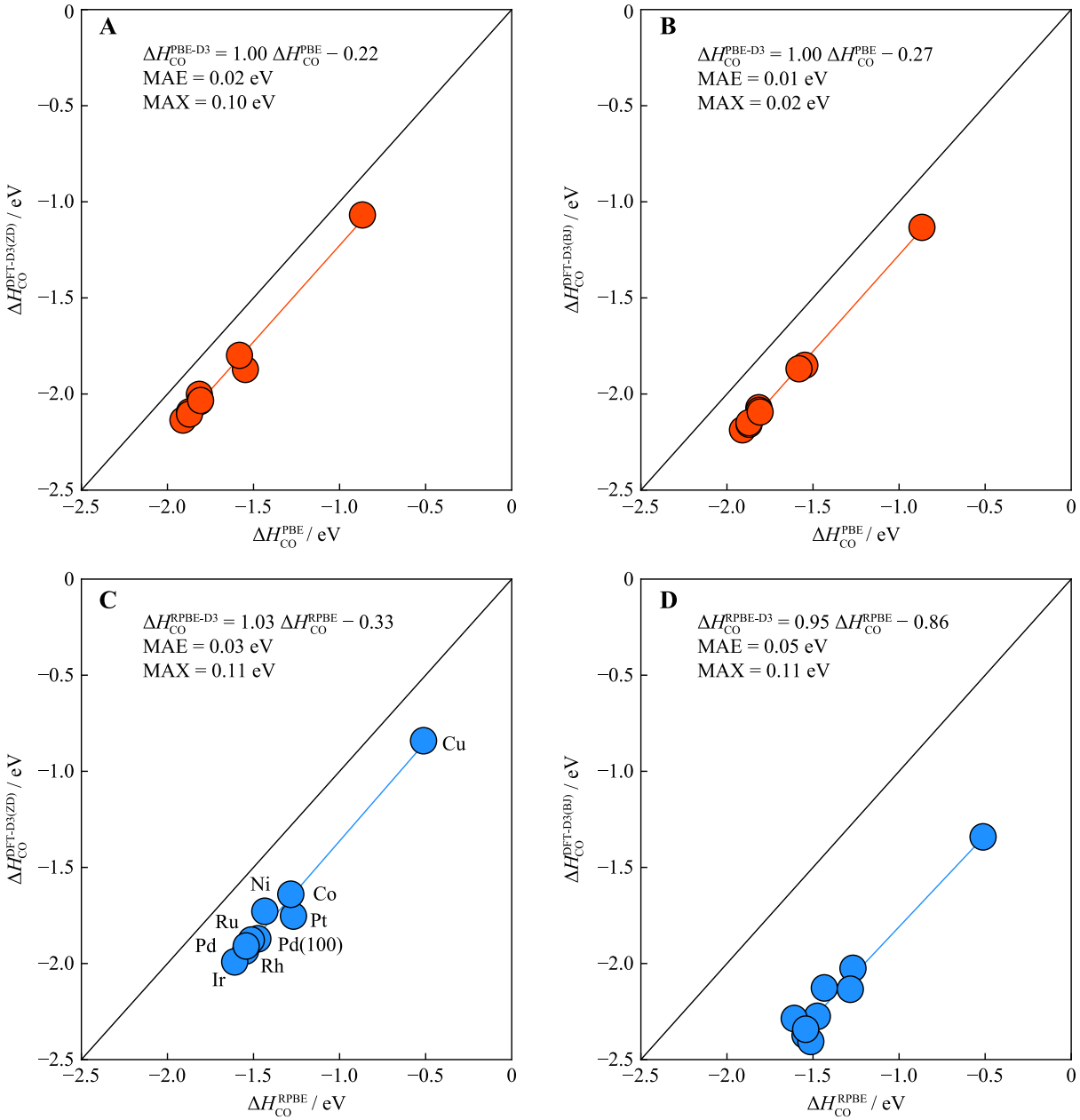


FIGURE 1 | Parity plot comparing the adsorption enthalpies of $CO_{(g)}$ on transition metals determined using the PBE and RPBE functionals and their D3-corrected versions: (A) PBE-D3(ZD); (B) PBE-D3(BJ); (C) RPBE-D3(ZD); and (D) RPBE-D3(BJ). In all panels, the regression equations are provided alongside the corresponding mean and maximum absolute errors (MAE and MAX, respectively).

products (the adsorbed phase) and reactants (the free molecule and clean metal surface) in $* + CO_{(g)} \rightarrow *CO$ entail similar errors and thus cancel out. This approximation may be particularly questionable for chemisorption processes on metals, where the chemical bonding environment of the free molecule changes drastically upon adsorption. For instance, although $CO_{(g)}$ exhibits discrete orbitals, *CO on transition metals exhibits broadened electronic states emerging from the hybridization of the CO orbitals with the metal bands [60–62]. This assumption of complete error cancellation during CO adsorption is illustrated in Figure 2A, where the errors associated with the reactants and products are represented by orange squares enclosing the compounds, alongside the resulting expression for the total error ($\varepsilon^{T} = 0$).

The significant errors reported above motivated us to formulate a strategy that corrects the energies of the free molecules using Equation (3) and assuming that error cancellation holds exclusively between the energies of the metal slab with and without the adsorbate ($\overline{\varepsilon_{CO}} = 0$), such that the total error is attributed solely to the gas phase ($\varepsilon^{T} = -\varepsilon_{CO(g)}$). Indeed, both the PBE and RPBE functionals have proven capable of reproducing experimental onset potentials for CO_2 electroreduction as well as activity trends for the $2e^{-}$ O_2 reduction reaction to H_2O_2 using this approximation [50, 63]. This approach is schematically illustrated in Figure 2B, where the gas-phase error is highlighted in red and the identical slab errors with and without the adsorbate are shown in orange.

30676630, 2026, 3, Downloaded from https://onlinelibrary.wiley.com/doi/10.1002/csc3.70031 by Technische Universitaet Wien, Wiley Online Library on [23/09/2026]. See the Terms and Conditions (https://onlinelibrary.wiley.com/terms-and-conditions) on Wiley Online Library for rules of use; OA articles are governed by the applicable Creative Commons License

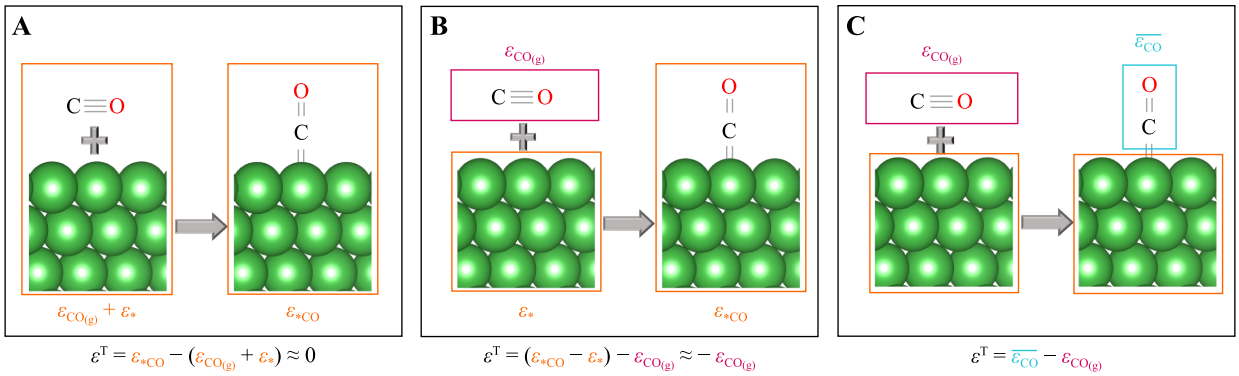


FIGURE 2 | Approximations to estimate the total error for CO adsorption on metals. (A) The DFT errors in the product and reactant energies are assumed to be similar (in orange). (B) Only the errors of the metal slab with and without the adsorbate are assumed to be similar (in orange); therefore, the $CO_{(g)}$ error (in red) is corrected. (C) The errors of the metal atoms in the slabs cancel out with and without the adsorbate (both shown in orange). Thus, the total error results from the gas-phase error of CO (ε_{CO}, in red) and the error in *CO ($\overline{\varepsilon_{CO}}$, in blue). In all cases, the resulting expression of the total error (ε^T) is shown.

A more rigorous treatment accounts explicitly for the error in the gas phase ($\varepsilon_{CO(g)} \neq 0$) while assuming complete error cancellation between the energies of the clean metal slab and the metal atoms not directly involved in bonding with the adsorbate, thus assigning an error to the adsorbate ($\overline{\varepsilon_{CO}} \neq 0$), see Figure 2C. Prior computational studies have shown that accounting for these two distinct errors unifies the results obtained with different functionals and aligns them with experimental observations [27, 28, 47, 64], thereby enhancing computational predictions.

To further assess the effect of D3 corrections on the computational modeling of CO adsorption, the three approaches outlined in Figure 2 were evaluated using the PBE and RPBE functionals, both with and without D3 (ZD) and D3 (BJ) corrections. The results are presented in Figure 3, where each approach is compared with the experimental enthalpies (ΔH_{CO}^{exp}) reported by Wellendorff et al. [48]. In Figure 3, the data obtained using PBE are displayed in the first row, whereas the data from RPBE are compiled in the second row. Each column corresponds to a distinct damping method for the dispersion corrections: the first column contains the results without dispersion corrections (without D3), the second shows the results with zero-damping corrections (D3 (ZD)), and the third presents the results incorporating the corrections using BJ damping (D3 (BJ)). Moreover, the red datapoints in each panel correspond to the scenario where complete error cancellation is assumed (DFT as is, see Figure 2A), the purple datapoints denote the gas-phase-corrected predictions (GPC; see Figure 2B), and the green datapoints represent enthalpies in which both the gas- and adsorbed-phase errors have been corrected (GPC + APC, see Figure 2C; APC: adsorbed-phase corrections). Briefly, the gas-phase corrections counteract the $CO_{(g)}$ error derived from the experimental formation enthalpy of $CO_{(g)}$ ($\varepsilon_{CO(g)}$, see Supporting Information S1: Note S1) [30], whereas adsorbed-phase corrections counteract the mean $\overline{\varepsilon_{CO}}$, which represents the average of the *CO error on all evaluated metals using the experimental enthalpies of adsorption [47, 48].

As illustrated in Figure 3A, the "DFT as is" enthalpies obtained with PBE are more negative than the experimental values by approximately 0.34 eV. This deviation is further exacerbated by D3 (ZD) and D3 (BJ) corrections, which yield considerably higher MAEs of 0.57 and 0.62 eV in Figure 3B,C, respectively. These observations indicate that dispersion corrections are disadvantageous for modeling CO adsorption on transition metals using the PBE functional. Gas-phase corrections markedly improve the predictive capability of PBE, as shown by the purple trends in Figure 3A–C; these corrected values align closer to the parity line, yielding lower MAEs of 0.11, 0.27, and 0.27 eV. Notably, removing the gas-phase errors isolates the adsorbed-phase errors as the only contribution, revealing that both PBE-D3 (ZD) and PBE-D3 (BJ) possess larger $\overline{\varepsilon_{CO}}$ values than plain PBE. Finally, when both the gas- and adsorbed-phase energies are corrected, the predicted enthalpies of PBE, PBE-D3 (ZD), and PBE-D3 (BJ) cluster closely along the parity line, exhibiting MAEs as low as 0.10 eV, which approach chemical accuracy (~0.04 eV). In summary, although the correction scheme outlined in Figure 2C is the most effective approach for minimizing the errors of PBE, PBE-D3 (ZD), and PBE-D3 (BJ), the scheme in Figure 2B serves as a reasonable approximation for plain PBE calculations but not for PBE-D3 (ZD) and PBE-D3 (BJ).

Regarding the RPBE functional, the plain RPBE enthalpies presented in Figure 3D exhibit remarkable agreement with experimental data, yielding a low MAE of 0.08 eV [17]. Conversely, RPBE-D3 (ZD) and RPBE-D3 (BJ) systematically shift the adsorption energies to more negative values, inducing severe deviations from experimental observations. Specifically, the MAE for RPBE-D3 (ZD) is 0.39 eV, whereas that of the RPBE-D3(BJ) is approximately the double, reaching 0.81 eV (Figure 3E,F). Gas-phase corrections slightly increase the MAE of the uncorrected RPBE from 0.08 to 0.11 eV, which indicates that the full error cancellation assumption shown in Figure 2A is well justified for this particular system, as no additional corrections are required to achieve accurate adsorption energies.

Furthermore, the gas-phase correction increases the MAE of the RPBE-D3 (ZD) functional by 0.01 eV (0.39 vs. 0.40 eV in Figure 3E), indicating that $\varepsilon_{CO_{(g)}}$ is negligible and that the total error is predominantly driven by errors in the adsorbed phase. Conversely, for RPBE-D3 (BJ), the gas-phase corrections noticeably reduce the MAE from 0.81 to 0.58 eV. Similar to the

30676630, 2026, 3, Downloaded from https://onlinelibrary.wiley.com/doi/10.1002/csc3.70031 by Technische Universitaet Wien, Wiley Online Library on [23/09/2026]. See the Terms and Conditions (https://onlinelibrary.wiley.com/terms-and-conditions) on Wiley Online Library for rules of use; OA articles are governed by the applicable Creative Commons License

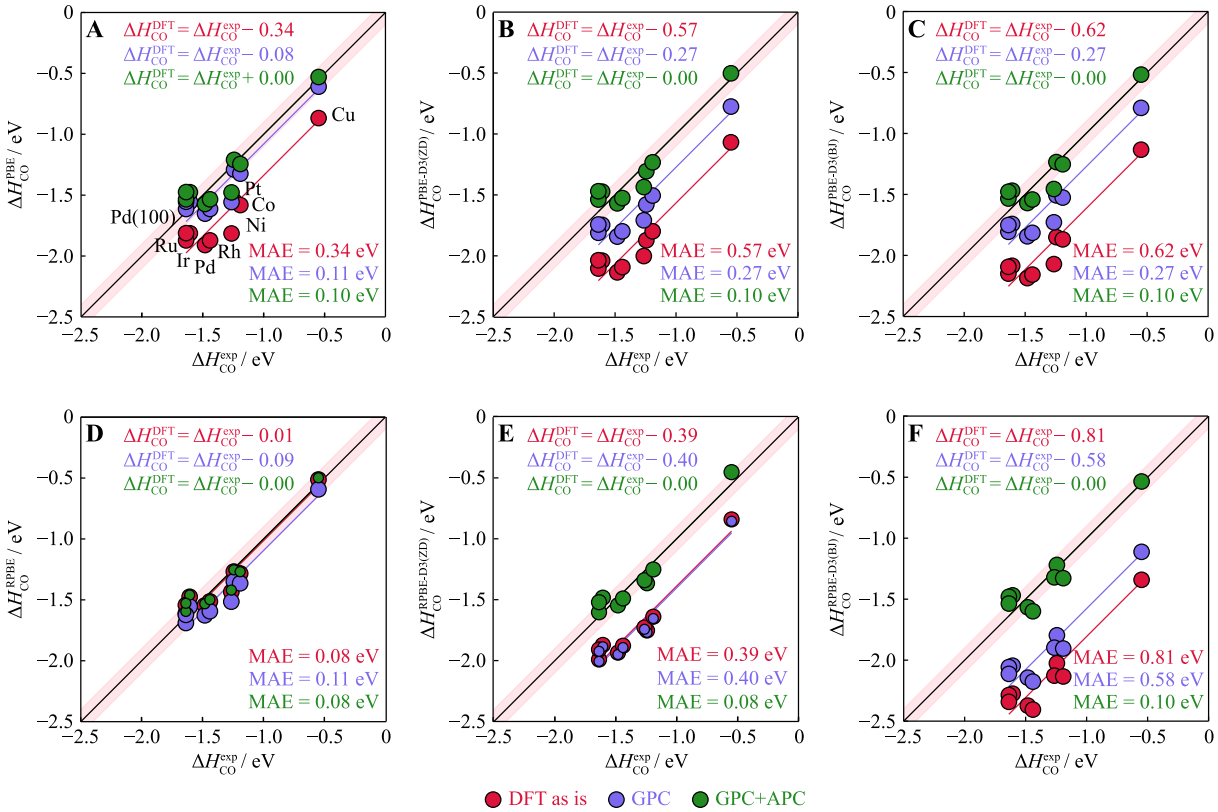


FIGURE 3 | DFT-calculated adsorption enthalpies of CO versus the experimental adsorption enthalpies of CO for (A) PBE, (B) PBE-D3(ZD), (C) PBE-D3(BJ), (D) RPBE, (E) RPBE-D3(ZD), and (F) RPBE-D3(BJ). Each panel incorporates different corrections: without energy rectification (DFT as is, in red), including only gas-phase corrections (GPC, in purple), and including both gas- and adsorbed-phase corrections (GPC + APC, in green). All panels show the regression fits and MAEs at each correction stage. The corresponding MAXs are listed in the Supporting Information S1: Table S11.

PBE functional, the addition of D3 (ZD) and D3 (BJ) corrections degrades the description of the adsorbed phase for RPBE, yielding MAEs of 0.40 and 0.58 eV compared to the value of 0.11 eV, corresponding to the uncorrected case (Figure 3D–F). Finally, when both the gas- and adsorbed-phase corrections are incorporated, the RPBE, RPBE-D3 (ZD), and RPBE-D3 (BJ) predictions achieve agreement with experimental values to within 0.10 eV across all cases.

Figure 3 reveals that the application of D3 corrections shifts both $\varepsilon_{CO_{(g)}}$ and $\overline{\varepsilon_{CO}}$ to varying degrees depending on the selected damping function. In turn, Figure 4 summarizes the tradeoff between the gas- and adsorbed-phase errors, which illustrates that only plain RPBE exhibits gas- and adsorbed-phase errors of similar magnitudes and identical signs, resulting in an effective cancellation of errors. In contrast, all other evaluated functionals exhibit large individual errors of opposite signs; consequently, their contributions accumulate rather than cancel, thereby increasing the magnitude of the total error. Supporting Information S1: Tables S7 and S9 list the calculated gas- and adsorbed-phase errors for each functional, whereas Supporting Information S1: Tables S3, S8, and S10 list the respective uncorrected, gas-phase corrected (GPC), and fully corrected (GPC + APC) adsorption enthalpies.

For completeness, we note that the present deconvolution scheme is specifically designed to isolate and eliminate systematic DFT errors. Alternatively, other methodologies in literature leverage error cancellation by means of isodesmic reactions for adsorbates [31]. Furthermore, a recent work used DFT+U [65] in combination with various functionals to examine CO adsorption on transition metals. The authors showed that functional- and atom-specific values of U applied to the *p* orbitals of C and O atoms help resolve the "CO puzzle" both qualitatively and quantitatively [21]. As detailed in Note S3 (Supporting Information S1: Table S13), PBE, PBE-D3, PBE-D3+U, RPBE, RPBE-D3, and RPBE-D3+U calculations were performed to evaluate CO adsorption on Pt (111). The site preference of *CO adsorption on Pt(111) is correctly reproduced when employing the PBE-D3+U and RPBE-D3+U formulations. For both functionals, the inclusion of the U term decreases the overbinding tendency observed in the corresponding D3 calculations. Although PBE-D3+U yields a lower error than plain PBE, RPBE-D3+U is less accurate than plain RPBE. In any case, the values of U should be optimized to simultaneously minimize both the gas- and adsorbed-phase errors, and the transferability of these paramaters to other C- and O-containing adsorbates remains an important target for future investigations.

3.3 | Error-Aware Adsorption Thermodynamics

Having systematically evaluated the differences in CO adsorption energies between DFT calculations and experimental benchmarks, it is instructive to look at them from a

30676630, 2026, 3, Downloaded from https://onlinelibrary.wiley.com/doi/10.1002/csc3.70031 by Technische Universitaet Wien, Wiley Online Library on [23/09/2026]. See the Terms and Conditions (https://onlinelibrary.wiley.com/terms-and-conditions) on Wiley Online Library for rules of use; OA articles are governed by the applicable Creative Commons License

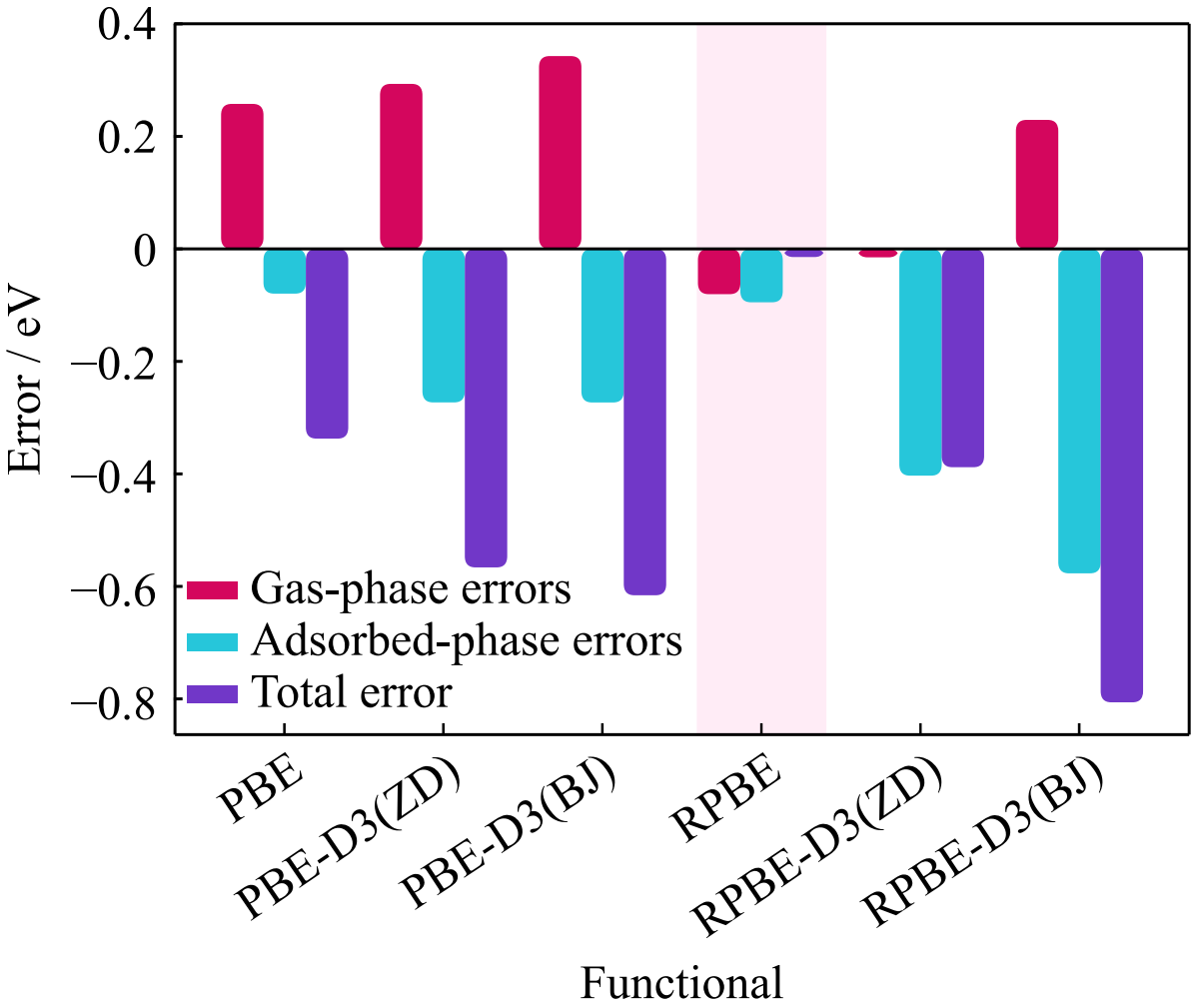


FIGURE 4 | Gas- (red) and adsorbed-phase (blue) errors calculated for PBE, RPBE, and their D3-corrected versions with two different damping functions. Because the difference between these two errors corresponds to the total error in the adsorption enthalpy (violet, see Equation (3)), error cancellation only occurs when the blue and red bars possess similar sizes and identical signs, as is the case for plain RPBE, which is highlighted in pink.

thermodynamic perspective. Figure 5 summarizes the effect of D3 corrections on $CO_{(g)}$ adsorption. The enthalpy diagrams include the states of $CO_{(g)}$ and *CO and use $C_{(s)} + \frac{1}{2}O_{2(g)} + *$ as a reference state. In Figure 5A, the experimental data for $CO_{(g)}$ and *CO adsorbed on Cu (represented by "*") are shown in green, whereas the enthalpies obtained with an arbitrary functional "XC" are shown in black. Copper was selected as a representative case study for this illustration due to its relevance in CO and CO_2 electrocatalytic reduction [4, 66]. Crucially, the reference state remains consistent between experimental measurements and computational models only when the DFT-calculated energy of $O_{2(g)}$ is corrected. Thus, all DFT-calculated energies in Figure 5 incorporate the well-documented gas-phase correction for $O_{2(g)}$ [67, 68] (Supporting Information S1: Note S1.1).

As the reference baseline in these enthalpy diagrams comprises the elements in their standard states alongside the free Cu(111) surface sites, the energy difference relative to the initial state ("$CO_{(g)} + *$") in Figure 5A is equivalent to the formation enthalpy of CO ($\Delta_f H_{CO_{(g)}}$). Accordingly, the distance from the origin to the second state ("*CO") represents the formation enthalpy of adsorbed CO ($\Delta_f H_{*CO}$). The difference between these two states yields the CO adsorption enthalpy ($\Delta H_{CO@Cu} = \Delta_f H_{*CO} - \Delta_f H_{CO_{(g)}}$). Moreover, the discrepancies between the experimental benchmarks and XC enthalpies reflect the gas- and adsorbed-phase errors. Specifically, the deviation between $\Delta_f H^{exp}_{CO_{(g)}}$ and $\Delta_f H^{XC}_{CO_{(g)}}$ amounts to the $CO_{(g)}$ error ($\varepsilon_{CO} = \Delta_f H^{XC}_{CO_{(g)}} - \Delta_f H^{exp}_{CO_{(g)}}$, in red in Figure 5), and the difference between the adsorbed-phase formation enthalpies, $\Delta_f H^{exp}_{*CO}$ and $\Delta_f H^{XC}_{*CO}$, is the adsorbed-phase error ($\overline{\varepsilon_{CO}} = \Delta_f H^{XC}_{*CO} - \Delta_f H^{exp}_{*CO}$, represented by cyan arrows). Supporting Information S1: Note S2 comprehensively details how ε_{CO} and $\overline{\varepsilon_{CO}}$ are related to the red and cyan arrows in Figure 5.

Figure 5B compares the experimental enthalpies with those calculated using PBE, PBE-D3 (ZD), and PBE-D3 (BJ). This figure reveals that the gas-phase predictions for PBE deviate from the experimental baseline by ~0.30 eV on average over Cu; conversely, the calculated formation enthalpies of *CO become more negative than the experimental data by approximately 0.24 eV upon introducing D3 corrections, which increases the adsorbed-phase error from −0.06 to −0.24 eV.

30676630, 2026, 3, Downloaded from https://onlinelibrary.wiley.com/doi/10.1002/csc3.70031 by Technische Universitaet Wien, Wiley Online Library on [23/09/2026]. See the Terms and Conditions (https://onlinelibrary.wiley.com/terms-and-conditions) on Wiley Online Library for rules of use; OA articles are governed by the applicable Creative Commons License

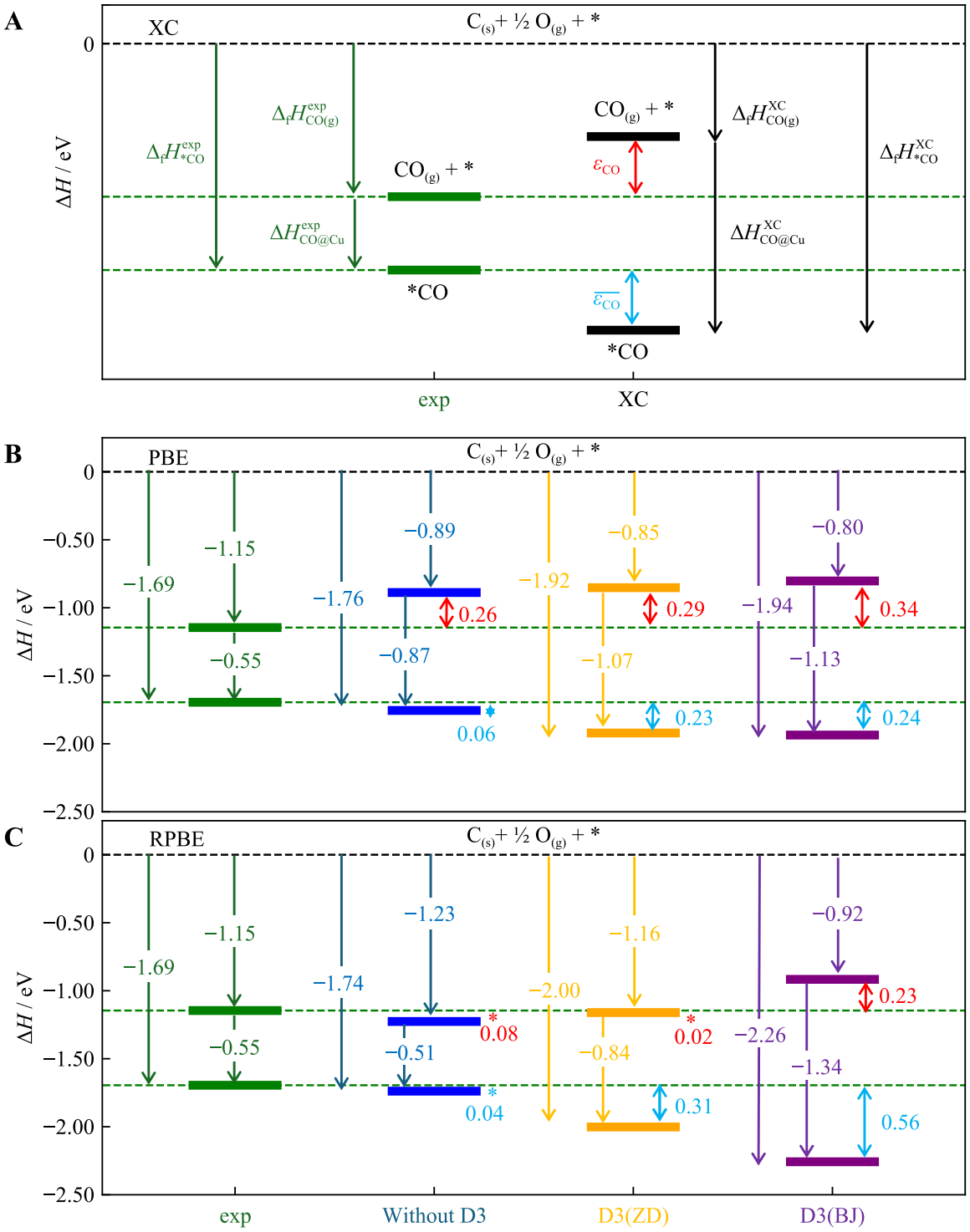


FIGURE 5 | Enthalpy diagram showing the overall effect of D3 dispersion corrections on CO adsorption on Cu(111). (A) Comparison between the experimental values ("exp") and predictions from an arbitrary functional XC. (B) Comparison between the experimental values and PBE predictions without D3 corrections ("Without D3") and with zero-damping (D3 (ZD)) and BJ-damping (D3 (BJ)) corrections for CO adsorption on Cu(111). (C) Comparison between the experimental values and RPBE predictions without D3 corrections ("Without D3") and with zero-damping (D3 (ZD)) and BJ-damping (D3 (BJ)) corrections for CO adsorption on Cu(111). The experimental (green), uncorrected (blue), D3 (ZD)-corrected (orange), and D3 (BJ)-corrected (purple) enthalpies are provided in each case. The differences between the predicted and experimental $CO_{(g)}$ formation enthalpies are depicted in red (ε_{CO}), and the differences between the predicted and experimental formation enthalpies of *CO are depicted in cyan ($\overline{\varepsilon_{CO}}$).

Furthermore, Figure 5C evaluates the results obtained for the RPBE functional. The CO formation enthalpies calculated using RPBE and RPBE-D3 (ZD) track the experimental benchmarks closely, exhibiting negligible errors. However, the incorporation of BJ damping produces a less negative gas-phase enthalpy value, thereby expanding the gas-phase error to 0.23 eV. Similar

30676630, 2026, 3, Downloaded from https://onlinelibrary.wiley.com/doi/10.1002/csc3.70031 by Technische Universitaet Wien, Wiley Online Library on [23/09/2026]. See the Terms and Conditions (https://onlinelibrary.wiley.com/terms-and-conditions) on Wiley Online Library for rules of use; OA articles are governed by the applicable Creative Commons License

to the trends identified for PBE, the application of D3 corrections results in overly negative *CO formation enthalpies on Cu, leading to larger adsorbed-phase errors than those of plain RPBE. Specifically, the overestimations introduced by zero and BJ damping lead to adsorbed-phase errors as large as −0.31 and −0.56 eV, which are in stark contrast with the small error of −0.04 eV obtained with plain RPBE.

4 | Conclusions

In this study, we investigated whether the use of dispersion corrections by default for adsorption energies is advisable. To address this question, the effects of two different D3 corrections (with zero and BJ damping) on the CO adsorption energies were systematically examined across eight transition metals (Ni, Pt, Pd, Ir, Rh, Cu, Co, and Ru). When employing the PBE and RPBE functionals, the inclusion of D3 corrections consistently yielded more negative adsorption energies relative to the plain functionals and experimental benchmarks.

As indicated by the MAEs presented in Figure 3, the deviations from experimental values obtained for PBE increased from 0.34 eV for the plain functional to 0.57 and 0.62 eV when zero-damping and BJ-damping D3 corrections were implemented, respectively. For RPBE, the introduction of D3 (ZD) and D3(BJ) corrections leads to an overstabilization of 0.39 and 0.81 eV relative to experimental data, contrasting sharply with the plain RPBE predictions, which deviate by only 0.08 eV.

To rationalize these trends, an error decomposition scheme was applied, which revealed a distinct functional-dependent impact of the D3 corrections. For PBE, the addition of D3 corrections results in only minor adjustments in the gas-phase error (0.26 vs. 0.29 vs. 0.34 eV; see Figures 4 and 5B and Supporting Information S1: Table S7), whereas the mean adsorbed-phase error increased by 0.19 eV, as evidenced by the purple offsets in Figure 3A–C (−0.08 vs. −0.27 vs. −0.27 eV; see Figure 4 and Supporting Information S1: Table S9). The effect is significantly more pronounced when examining the RPBE functional: The gas-phase error changes marginally with the inclusion of zero damping corrections (−0.08 vs. −0.02 eV in Figures 4 and 5C) but expands to 0.23 eV when BJ damping is applied. Furthermore, the mean adsorbed-phase error calculated across the eight transition metals (reflected by the purple offsets in Figures 3D–F and 4) increases substantially relative to the uncorrected RPBE baseline: −0.09 versus −0.40 eV for zero damping and −0.58 eV for BJ damping.

These findings indicate that (1) RPBE, the prototypical functional for CO adsorption modeling, exhibits a higher sensitivity to D3 corrections than the PBE functional, and (2) BJ damping consistently induces larger gas- and adsorbed-phase errors than zero-damped or as is DFT calculations. Only when the gas-phase energies are fully corrected and the corresponding adsorbed-phase energies are corrected using a mean value across metals do the DFT predictions align with experimental data within the limits of chemical accuracy, regardless of the underlying functional and damping scheme selected.

Collectively, these results shed light on a frequently overlooked pitfall in catalysis modeling: D3 dispersion corrections should be added when strictly necessary, not by default. We hope this work prompts computational chemists to become more aware of the thermochemical errors present in the DFT calculations of molecules and adsorbates and how they may mislead catalytic models by predicting inaccurate adsorption energies.

Author Contributions

All authors actively contributed to the research that led to this paper, discussed the results, and participated in the writing of the manuscript.

Acknowledgments

We acknowledge the financial support from grants PID2021-127957NB-I00 and PID2024-158557OB-C22, which are funded by the Spanish MCIN/AEI/10.13039/501100011033 and the European Social Fund Plus (ESF+). Federico Calle-Vallejo and Stefan Kurth also acknowledge the financial support from the Basque Government via the Elkartek program (Project title CICe2025 and Grant No. KK2025-00054). Finally, we thank Red Española de Supercomputación (RES) for time at MareNostrum5 and Turgalium (Project Codes QHS-2024-3-0025, QHS-2025-1-0024, QHS-2025-2-0044, QHS-2025-3-0029, and QHS-2026-1-0045). The authors thank SGIker's Scientific Computing Service (EHU/FEDER, EU) for the technical and human support.

Conflicts of Interest

The authors declare no conflicts of interest.

Data Availability Statement

The data that support the findings of this study are available from the corresponding author upon reasonable request.

References

1. M. Behrens, F. Studt, I. Kasatkin, et al., "The Active Site of Methanol Synthesis Over $Cu/ZnO/Al_2O_3$ Industrial Catalysts," *Science* 336, no. 6083 (2012): 893–897, https://doi.org/10.1126/science.1219831.

2. M. Ojeda, R. Nabar, A. U. Nilekar, A. Ishikawa, M. Mavrikakis, and E. Iglesia, "CO Activation Pathways and the Mechanism of Fischer–Tropsch Synthesis," *Journal of Catalysis* 272, no. 2 (2010): 287–297, https://doi.org/10.1016/j.jcat.2010.04.012.

3. A. A. Gokhale, J. A. Dumesic, and M. Mavrikakis, "On the Mechanism of Low-Temperature Water Gas Shift Reaction on Copper," *Journal of the American Chemical Society* 130, no. 4 (2008): 1402–1414, https://doi.org/10.1021/ja0768237.

4. S. Nitopi, E. Bertheussen, S. B. Scott, et al., "Progress and Perspectives of Electrochemical CO_2 Reduction on Copper in Aqueous Electrolyte," *Chemical Reviews* 119, no. 12 (2019): 7610–7672, https://doi.org/10.1021/acs.chemrev.8b00705.

5. C. W. Li, J. Ciston, and M. W. Kanan, "Electroreduction of Carbon Monoxide to Liquid Fuel on Oxide-Derived Nanocrystalline Copper," *Nature* 508, no. 7497 (2014): 504–507, https://doi.org/10.1038/nature13249.

6. F. Calle-Vallejo, M. D. Pohl, and A. S. Bandarenka, "Quantitative Coordination–Activity Relations for the Design of Enhanced Pt Catalysts for CO Electro-Oxidation," *ACS Catalysis* 7, no. 7 (2017): 4355–4359, https://doi.org/10.1021/acscatal.7b01105.

7. N. P. Lebedeva, M. T. M. Koper, E. Herrero, J. M. Feliu, and R. A. van Santen, "Cooxidation on Stepped Pt [(n111) × (111)] Electrodes," *Journal of Electroanalytical Chemistry* 487, no. 1 (2000): 37–44, https://doi.org/10.1016/S0022-0728(00)00149-2.

30676630, 2026, 3, Downloaded from https://onlinelibrary.wiley.com/doi/10.1002/csc3.70031 by Technische Universitaet Wien, Wiley Online Library on [23/09/2026]. See the Terms and Conditions (https://onlinelibrary.wiley.com/terms-and-conditions) on Wiley Online Library for rules of use; OA articles are governed by the applicable Creative Commons License

8. N. P. Lebedeva, M. T. M. Koper, J. M. Feliu, and R. A. van Santen, "Role of Crystalline Defects in Electrocatalysis: Mechanism and Kinetics of CO Adlayer Oxidation on Stepped Platinum Electrodes," *Journal of Physical Chemistry B* 106, no. 50 (2002): 12938–12947, https://doi.org/10.1021/jp0204105.

9. M. Z. F. Kamarudin, S. K. Kamarudin, M. S. Masdar, and W. R. W. Daud, "Review: Direct Ethanol Fuel Cells," *International Journal of Hydrogen Energy* 38, no. 22 (2013): 9438–9453, https://doi.org/10.1016/j.ijhydene.2012.07.059.

10. A. Hamnett, "Mechanism and Electrocatalysis in the Direct Methanol Fuel Cell," *Catalysis Today* 38, no. 4 (1997): 445–457, https://doi.org/10.1016/S0920-5861(97)00054-0.

11. J. Rossmeisl, P. Ferrin, G. A. Tritsaris, et al., "Bifunctional Anode Catalysts for Direct Methanol Fuel Cells," *Energy & Environmental Science* 5, no. 8 (2012): 8335, https://doi.org/10.1039/c2ee21455e.

12. J. K. Nørskov, F. Abild-Pedersen, F. Studt, and T. Bligaard, "Density Functional Theory in Surface Chemistry and Catalysis," *Proceedings of the National Academy of Sciences of the United States of America* 108, no. 3 (2011): 937–943, https://doi.org/10.1073/pnas.1006652108.

13. K. Burke, "Perspective on Density Functional Theory," *Journal of Chemical Physics* 136, no. 15 (2012): 150901, https://doi.org/10.1063/1.4704546.

14. K. Capelle, "A Bird's-eye View of Density-Functional Theory," *Brazilian Journal of Physics* 36, no. 4a (2006): 1318–1343, https://doi.org/10.1590/S0103-97332006000700035.

15. N. Mardirossian and M. Head-Gordon, "Thirty Years of Density Functional Theory in Computational Chemistry: An Overview and Extensive Assessment of 200 Density Functionals," *Molecular Physics* 115, no. 19 (2017): 2315–2372, https://doi.org/10.1080/00268976.2017.1333644.

16. J. P. Perdew, K. Burke, and M. Ernzerhof, "Generalized Gradient Approximation Made Simple," *Physical Review Letters* 77, no. 18 (1996): 3865–3868, https://doi.org/10.1103/PhysRevLett.77.3865.

17. B. Hammer, L. B. Hansen, and J. K. Nørskov, "Improved Adsorption Energetics Within Density-Functional Theory Using Revised Perdew-Burke-Ernzerhof Functionals," *Physical Review B* 59, no. 11 (1999): 7413–7421, https://doi.org/10.1103/PhysRevB.59.7413.

18. J. Wellendorff, K. T. Lundgaard, A. Møgelhøj, et al., "Density Functionals for Surface Science: Exchange-Correlation Model Development With Bayesian Error Estimation," *Physical Review B* 85, no. 23 (2012): 235149, https://doi.org/10.1103/PhysRevB.85.235149.

19. P. J. Feibelman, B. Hammer, J. K. Nørskov, et al., "The CO/Pt(111) Puzzle," *Journal of Physical Chemistry B* 105, no. 18 (2001): 4018–4025, https://doi.org/10.1021/jp002302t.

20. P. Janthon, F. Viñes, J. Sirijaraensre, J. Limtrakul, and F. Illas, "Adding Pieces to the CO/Pt(111) Puzzle: The Role of Dispersion," *Journal of Physical Chemistry C* 121, no. 7 (2017): 3970–3977, https://doi.org/10.1021/acs.jpcc.7b00365.

21. T. Maxson and T. Szilvási, "Self-Consistent DFT+U for CO Adsorption on Transition Metal Surfaces: A Practical Correction and Benchmark," *Journal of Catalysis* 458 (2026): 116875, https://doi.org/10.1016/j.jcat.2026.116875.

22. L. Schimka, J. Harl, A. Stroppa, et al., "Accurate Surface and Adsorption Energies From Many-Body Perturbation Theory," *Nature Materials* 9, no. 9 (2010): 741–744, https://doi.org/10.1038/nmat2806.

23. S. Kurth, J. P. Perdew, and P. Blaha, "Molecular and Solid-State Tests of Density Functional Approximations: LSD, GGAs, and Meta-GGAs," *International Journal of Quantum Chemistry* 75, no. 4–5 (1999): 889–909, https://doi.org/10.1002/(SICI)1097-461X(1999)75:4/5<889::AID-QUA54>3.0.CO;2-8.

24. L. Wang, T. Maxisch, and G. Ceder, "Oxidation Energies of Transition Metal Oxides Within the GGA + U Framework," *Physical Review B* 73, no. 19 (2006): 195107, https://doi.org/10.1103/PhysRevB.73.195107.

25. F. Calle-Vallejo, J. I. Martínez, J. M. García-Lastra, M. Mogensen, and J. Rossmeisl, "Trends in Stability of Perovskite Oxides," *Angewandte Chemie International Edition* 49, no. 42 (2010): 7699–7701, https://doi.org/10.1002/anie.201002301.

26. J. I. Martínez, H. A. Hansen, J. Rossmeisl, and J. K. Nørskov, "Formation Energies of Rutile Metal Dioxides Using Density Functional Theory," *Physical Review B* 79, no. 4 (2009): 045120, https://doi.org/10.1103/PhysRevB.79.045120.

27. E. Romeo, F. T. You, H. B. Ma, F. Illas, B. S. Yeo, and F. Calle-Vallejo, "Improving the Description of Adsorbed Hydroxyl to Make Predictive Catalytic Activity Models," *ACS Catalysis* 15, no. 21 (2025): 18004–18012, https://doi.org/10.1021/acscatal.5c04121.

28. L. G. V. Briquet, M. Sarwar, J. Mugo, G. Jones, and F. Calle-Vallejo, "A New Type of Scaling Relations to Assess the Accuracy of Computational Predictions of Catalytic Activities Applied to the Oxygen Evolution Reaction," *ChemCatChem* 9, no. 7 (2017): 1261–1268, https://doi.org/10.1002/cctc.201601662.

29. A. Kiejna, G. Kresse, J. Rogal, A. De Sarkar, K. Reuter, and M. Scheffler, "Comparison of the Full-Potential and Frozen-Core Approximation Approaches to Density-Functional Calculations of Surfaces," *Physical Review B* 73, no. 3 (2006): 035404, https://doi.org/10.1103/PhysRevB.73.035404.

30. R. Urrego-Ortiz, S. Builes, F. Illas, and F. Calle-Vallejo, "Gas-Phase Errors in Computational Electrocatalysis: A Review," *EES Catalysis* 2, no. 1 (2024): 157–179, https://doi.org/10.1039/d3ey00126a.

31. B. Kreitz, K. Abeywardane, and C. F. Goldsmith, "Linking Experimental and Ab Initio Thermochemistry of Adsorbates With a Generalized Thermochemical Hierarchy," *Journal of Chemical Theory and Computation* 19, no. 13 (2023): 4149–4162, https://doi.org/10.1021/acs.jctc.3c00112.

32. J. Hermann, R. A. DiStasio Jr, and A. Tkatchenko, "First-Principles Models for Van Der Waals Interactions in Molecules and Materials: Concepts, Theory, and Applications," *Chemical Reviews* 117, no. 6 (2017): 4714–4758, https://doi.org/10.1021/acs.chemrev.6b00446.

33. S. Grimme, S. Ehrlich, and L. Goerigk, "Effect of the Damping Function in Dispersion Corrected Density Functional Theory," *Journal of Computational Chemistry* 32, no. 7 (2011): 1456–1465, https://doi.org/10.1002/jcc.21759.

34. S. Grimme, "Semiempirical GGA-Type Density Functional Constructed With a Long-Range Dispersion Correction," *Journal of Computational Chemistry* 27, no. 15 (2006): 1787–1799, https://doi.org/10.1002/jcc.20495.

35. E. Caldeweyher, S. Ehlert, A. Hansen, et al., "A Generally Applicable Atomic-Charge Dependent London Dispersion Correction," *Journal of Chemical Physics* 150, no. 15 (2019): 154122, https://doi.org/10.1063/1.5090222.

36. S. Grimme, "Accurate Description of Van Der Waals Complexes by Density Functional Theory Including Empirical Corrections," *Journal of Computational Chemistry* 25, no. 12 (2004): 1463–1473, https://doi.org/10.1002/jcc.20078.

37. S. Grimme, J. Antony, S. Ehrlich, and H. Krieg, "A Consistent and Accurate Ab Initio Parametrization of Density Functional Dispersion Correction (DFT-D) for the 94 Elements H-Pu," *Journal of Chemical Physics* 132, no. 15 (2010): 154104, https://doi.org/10.1063/1.3382344.

38. A. Tkatchenko, "Current Understanding of Van Der Waals Effects in Realistic Materials," *Advanced Functional Materials* 25, no. 13 (2015): 2054–2061, https://doi.org/10.1002/adfm.201403029.

30676630, 2026, 3, Downloaded from https://onlinelibrary.wiley.com/doi/10.1002/csc3.70031 by Technische Universitaet Wien, Wiley Online Library on [23/09/2026]. See the Terms and Conditions (https://onlinelibrary.wiley.com/terms-and-conditions) on Wiley Online Library for rules of use; OA articles are governed by the applicable Creative Commons License

39. S. K. Mitro, J. Brauer, and M. Fischer, "Benchmarking DFT Calculations for Adsorption Studies: Pharmaceuticals and Related Organic Molecules in Cation-Exchanged Zeolites," *Journal of Physical Chemistry C* 129, no. 46 (2025): 20722–20737, https://doi.org/10.1021/acs.jpcc.5c05270.

40. U. Yoon, K. Jeong, and S. H. Kim, "Advancing Electrocatalysis Through Density Functional Theory: From Reaction Mechanisms to Machine Learning Integration," *Journal of CO2 Utilization* 101 (2025): 103192, https://doi.org/10.1016/j.jcou.2025.103192.

41. G. Kresse and J. Furthmüller, "Efficient Iterative Schemes for Ab Initio Total-Energy Calculations Using a Plane-Wave Basis Set," *Physical Review B* 54, no. 16 (1996): 11169–11186, https://doi.org/10.1103/PhysRevB.54.11169.

42. J. Hafner, "Ab-Initio Simulations of Materials Using VASP: Density-Functional Theory and Beyond," *Journal of Computational Chemistry* 29, no. 13 (2008): 2044–2078, https://doi.org/10.1002/jcc.21057.

43. P. E. Blöchl, "Projector Augmented-Wave Method," *Physical Review B* 50, no. 24 (1994): 17953–17979, https://doi.org/10.1103/PhysRevB.50.17953.

44. G. Kresse and D. Joubert, "From Ultrasoft Pseudopotentials to the Projector Augmented-Wave Method," *Physical Review B* 59, no. 3 (1999): 1758–1775, https://doi.org/10.1103/PhysRevB.59.1758.

45. H. J. Monkhorst and J. D. Pack, "Special Points for Brillouin-Zone Integrations," *Physical Review B* 13, no. 12 (1976): 5188–5192, https://doi.org/10.1103/PhysRevB.13.5188.

46. M. Methfessel and A. T. Paxton, "High-Precision Sampling for Brillouin-Zone Integration in Metals," *Physical Review B* 40, no. 6 (1989): 3616–3621, https://doi.org/10.1103/PhysRevB.40.3616.

47. R. Urrego-Ortiz, C. S. Zhong, W. J. Teh, S. Builes, B. S. Yeo, and F. Calle-Vallejo, "Correcting Errors in the Adsorbed Intermediates of CO_2 Electroreduction," *Carbon Energy* 8, no. 2 (2026): e70128, https://doi.org/10.1002/cey2.70128.

48. J. Wellendorff, T. L. Silbaugh, D. Garcia-Pintos, et al., "A Benchmark Database for Adsorption Bond Energies to Transition Metal Surfaces and Comparison to Selected DFT Functionals," *Surface Science* 640 (2015): 36–44, https://doi.org/10.1016/j.susc.2015.03.023.

49. R. Urrego-Ortiz, S. Builes, F. Illas, S. T. Bromley, M. C. Figueiredo, and F. Calle-Vallejo, "Minimum Conditions for Accurate Modeling of Urea Production via Co-Electrolysis," *Communications Chemistry* 6, no. 1 (2023): 196, https://doi.org/10.1038/s42004-023-00990-7.

50. L. P. Granda-Marulanda, A. Rendón-Calle, S. Builes, F. Illas, M. T. M. Koper, and F. Calle-Vallejo, "A Semiempirical Method to Detect and Correct DFT-Based Gas-Phase Errors and Its Application in Electrocatalysis," *ACS Catalysis* 10, no. 12 (2020): 6900–6907, https://doi.org/10.1021/acscatal.0c01075.

51. R. Urrego-Ortiz, S. Builes, and F. Calle-Vallejo, "Automated Versus Chemically Intuitive Deconvolution of Density Functional Theory (DFT)-Based Gas-Phase Errors in Nitrogen Compounds," *Industrial & Engineering Chemistry Research* 61, no. 36 (2022): 13375–13382, https://doi.org/10.1021/acs.iecr.2c02111.

52. R. Urrego-Ortiz, S. Builes, and F. Calle-Vallejo, "Fast Correction of Errors in the DFT-Calculated Energies of Gaseous Nitrogen-Containing Species," *ChemCatChem* 13, no. 10 (2021): 2508–2516, https://doi.org/10.1002/cctc.202100125.

53. W. Wang, S. Y. Dai, X. D. Li, J. R. Yang, D. J. Srolovitz, and Q. S. Zheng, "Measurement of the Cleavage Energy of Graphite," *Nature Communications* 6, no. 1 (2015): 7853, https://doi.org/10.1038/ncomms8853.

54. K. Forster-Tonigold and A. Groß, "Dispersion Corrected RPBE Studies of Liquid Water," *Journal of Chemical Physics* 141, no. 6 (2014): 064501, https://doi.org/10.1063/1.4892400.

55. K. Tonigold and A. Groß, "Dispersive Interactions in Water Bilayers at Metallic Surfaces: A Comparison of the PBE and RPBE Functional Including Semiempirical Dispersion Corrections," *Journal of Computational Chemistry* 33, no. 6 (2012): 695–701, https://doi.org/10.1002/jcc.22900.

56. E. Romeo, F. Illas, and F. Calle-Vallejo, "Evaluating Adsorbate–Solvent Interactions: Are Dispersion Corrections Necessary," *Journal of Physical Chemistry C* 127, no. 21 (2023): 10134–10139, https://doi.org/10.1021/acs.jpcc.3c02934.

57. M. Vanin, J. J. Mortensen, A. K. Kelkkanen, J. M. Garcia-Lastra, K. S. Thygesen, and K. W. Jacobsen, "Graphene on Metals: A Van Der Waals Density Functional Study," *Physical Review B* 81, no. 8 (2010): 081408, https://doi.org/10.1103/PhysRevB.81.081408.

58. N. Arulmozhi, S. Hanselman, V. Tudor, et al., "Energetics and Kinetics of Hydrogen Electrosorption on a Graphene-Covered Pt(111) Electrode," *JACS Au* 3, no. 2 (2023): 526–535, https://doi.org/10.1021/jacsau.2c00648.

59. L. P. Granda-Marulanda, S. Builes, M. T. M. Koper, and F. Calle-Vallejo, "Influence of Van Der Waals Interactions on the Solvation Energies of Adsorbates at Pt-Based Electrocatalysts," *ChemPhysChem* 20, no. 22 (2019): 2968–2972, https://doi.org/10.1002/cphc.201900512.

60. B. Hammer and J. K. Nørskov, "Electronic Factors Determining the Reactivity of Metal Surfaces," *Surface Science* 343, no. 3 (1995): 211–220, https://doi.org/10.1016/0039-6028(96)80007-0.

61. B. Hammer and J. K. Nørskov, "Theoretical Surface Science and Catalysis—Calculations and Concepts," *Advances in Catalysis* 45 (2000): 71–129, https://doi.org/10.1016/S0360-0564(02)45013-4.

62. B. Hammer, Y. Morikawa, and J. K. Nørskov, "CO Chemisorption at Metal Surfaces and Overlayers," *Physical Review Letters* 76, no. 12 (1996): 2141–2144, https://doi.org/10.1103/PhysRevLett.76.2141.

63. R. Urrego-Ortiz, M. O. Almeida, and F. Calle-Vallejo, "Error Awareness in the Volcano Plots of Oxygen Electroreduction to Hydrogen Peroxide," *ChemSusChem* 17, no. 23 (2024): e202400873, https://doi.org/10.1002/cssc.202400873.

64. R. Christensen, H. A. Hansen, C. F. Dickens, J. K. Nørskov, and T. Vegge, "Functional Independent Scaling Relation for ORR/OER Catalysts," *Journal of Physical Chemistry C* 120, no. 43 (2016): 24910–24916, https://doi.org/10.1021/acs.jpcc.6b09141.

65. S. L. Dudarev, G. A. Botton, S. Y. Savrasov, C. J. Humphreys, and A. P. Sutton, "Electron-Energy-Loss Spectra and the Structural Stability of Nickel Oxide: An LSDA+U Study," *Physical Review B* 57, no. 3 (1998): 1505–1509, https://doi.org/10.1103/PhysRevB.57.1505.

66. A. Rendón-Calle, S. Builes, and F. Calle-Vallejo, "A Brief Review of the Computational Modeling of CO_2 Electroreduction on Cu Electrodes," *Current Opinion in Electrochemistry* 9 (2018): 158–165, https://doi.org/10.1016/j.coelec.2018.03.012.

67. J. K. Nørskov, J. Rossmeisl, A. Logadottir, et al., "Origin of the Overpotential for Oxygen Reduction at a Fuel-Cell Cathode," *Journal of Physical Chemistry B* 108, no. 46 (2004): 17886–17892, https://doi.org/10.1021/jp047349j.

68. E. Sargeant, F. Illas, P. Rodríguez, and F. Calle-Vallejo, "Importance of the Gas-Phase Error Correction for O_2 When Using DFT to Model the Oxygen Reduction and Evolution Reactions," *Journal of Electroanalytical Chemistry* 896 (2021): 115178, https://doi.org/10.1016/j.jelechem.2021.115178.

Supporting Information

Additional supporting information can be found online in the Supporting Information section.

Supporting Information S1: csc370031-sup-0001-suppl-data.docx.

30676630, 2026, 3, Downloaded from https://onlinelibrary.wiley.com/doi/10.1002/csc3.70031 by Technische Universitaet Wien, Wiley Online Library on [23/09/2026]. See the Terms and Conditions (https://onlinelibrary.wiley.com/terms-and-conditions) on Wiley Online Library for rules of use; OA articles are governed by the applicable Creative Commons License